Effect of the active metals on the selective H₂ production in glycerol steam reforming

M. Araque [a,b], L.M. Martínez T [a], J.C. Vargas [b], M.A. Centeno [c], A.C. Roger [a,*]

[a] Laboratoire des Matériaux, Surfaces et Procédés pour la Catalyse LMSPC, équipe "Energie et Carburants pour un Environnement Durable", UMR CNRS 7515, ECPM – Université de Strasbourg, 25 rue Becquerel, 67087 Strasbourg Cedex 2, France
[b] Departamento de Ingeniería Química y Ambiental, Universidad Nacional de Colombia Ciudad Universitaria, Avenida Carrera 30 N° 45-03, Edificio 453, Bogotá D.C., Colombia
[c] Instituto de Ciencia de Materiales de Sevilla. Centro mixto CSIC – Universidad de Sevilla, Avda. Américo Vespucio 49, 41092 Sevilla, Spain

A B S T R A C T

The production of hydrogen by glycerol steam reforming was studied using CeZr(Co, CoRh) catalysts. The effect of Co and Rh presence on the properties of the mixed oxides and the effect on the catalytic behavior were considered. The catalysts were characterized before and after testing by XRD, Raman, TPR, H₂-TPD, TPD-TPO and HRTEM. It was observed that the presence of Co allowed the selective H₂ production related with the presence of a metallic phase at the beginning of the reaction. The presence of Rh favored even more the H₂ production and also increased the stability of the catalyst. For CeZrCoRh, the presence of both metals enhanced the catalyst reduction capacity, a characteristic that significantly improved the catalytic behavior for glycerol steam reforming. The selective H₂ production was related to the capacity of the catalyst to activate H₂O under the reaction conditions. The progressive loss of this capacity decreases the production of H₂, and glycerol decomposition is actually favored over glycerol steam reforming. According to the initial distribution of products, and its evolution with time on stream, two main reaction pathways were proposed.
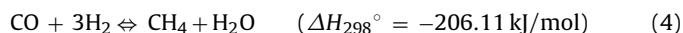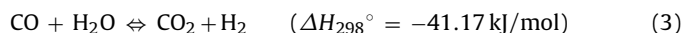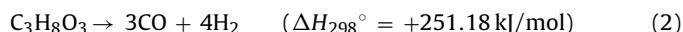
© 2012 Elsevier B.V. All rights reserved.

1. Introduction

Glycerol is largely generated as the principal co-product in the production of biodiesel by the transesterification process with alcohols. Due to the increase in the production of biodiesel several alternatives are proposed for the crude glycerol valorization [1]. The use of hydrogen as an energy vector represents one of these alternatives, ensuring the production of H₂ from renewable resources, sustainability required by the "hydrogen economy".

Glycerol steam reforming (GSR) proceeds according to the following reaction:

$$C_3H_8O_3 + 3H_2O \rightarrow 3CO_2 + 7H_2 \qquad (\Delta H_{298}^{\circ} = +123\,kJ/mol) \quad (1)$$

CO and CH₄ have also been observed as reaction products [2,3], and their production has been related to glycerol decomposition (Reaction (2)), water-gas shift reaction (Reaction (3)) and methanation reaction (Reaction (4)):

$$C_3H_8O_3 \rightarrow 3CO + 4H_2 \qquad (\Delta H_{298}^{\circ} = +251.18\,kJ/mol) \quad (2)$$

$$CO + H_2O \Leftrightarrow CO_2 + H_2 \qquad (\Delta H_{298}^{\circ} = -41.17\,kJ/mol) \quad (3)$$

$$CO + 3H_2 \Leftrightarrow CH_4 + H_2O \qquad (\Delta H_{298}^{\circ} = -206.11\,kJ/mol) \quad (4)$$

In GSR several studies have been performed [4]. High H₂ productions and glycerol conversions have been observed using Ru/Y₂O₃ at 600 °C [5], Ir/CeO₂ at 400 °C [6], and Ni and Rh supported catalysts at 900 °C [7,8]. However, the formation of carbon deposits and deactivation of the catalysts remain as an unsolved problem [4]. Therefore a catalyst that promotes carbon deposit gasification and that will be active for the WGS reaction is required to preserve the initial activity of the catalyst.

In previous works we have already reported satisfactory activity and selectivity to H₂ production using Ce-Zr-Co and Ce-Zr-Co-Rh catalysts [9]. The effect of the reaction temperature and the presence of Rh were studied for 35 wt% glycerol feed solution, obtaining during the first hours of reaction H₂ yields of 5.7 (81%) and 6.7 (96%) $molH_2\,mol_{Gly.in}^{-1}$, respectively. The stability of the catalysts was considerably promoted by the presence of Rh, but after 16 h hours the catalyst's activity decreased anyways. The formation of different carbon deposits were observed for both catalysts after reaction. In recent works on Ni based catalysts [10] the stability of the catalyst was related to a strong metal-support interaction: for Ni/ZrO₂ catalyst, stable glycerol conversion (72%) and H₂ yield (65%) were obtained at 650 °C for 20 h. At this temperature no coke formation was detected after reaction for this catalyst, may be due to the low glycerol feed concentration of 10 wt%. Dave and Pant

* Corresponding author.
  E-mail address: annececile.roger@unistra.fr (A.C. Roger).

[11], also reported stable glycerol conversion (100%) and H_2 yield ($4 \, mol \, H_2 \, mol_{Gly.in}{}^{-1}$, approximately) for 14 h at 700 °C. The catalyst used was a Ni supported on ZrO_2/CeO_2 with a 10 wt% glycerol feed. After reaction, low amounts of coke were observed (0.8 wt%), correlated by the authors to the promoted gasification capacity induced by CeO_2.

According to the previous works, the Ce-Zr-Co mixed oxides presented good performances for H_2 production by glycerol steam reforming. In this paper we attempt to clarify the beneficial effect of Rh in Ce-Zr and Ce-Zr-Co mixed oxides. The changes in the structural and redox characteristics of CeZr, CeZrRh, CeZrCo and CeZrCoRh were determined and related to the catalytic behavior. The role of the catalysts and a scheme of reaction pathways were then proposed according to the reactivity results.

2. Experimental

2.1. Preparation of the catalysts

Fluorite mixed oxides catalysts were synthesized using the pseudo sol-gel method based on the thermal decomposition of metallic propionates [12–14]. The starting salts were cerium (III) acetate hydrate, zirconium (IV) acetylacetonate, cobalt (II) acetate and rhodium (II) acetate. The salts were dissolved separately in propionic acid with a concentration of $0.12 \, mol \, L^{-1}$. The solutions were mixed at 80 °C for 1 h and the solvent was evaporated until a resin was obtained. Finally, the resin was heated at 2 °C min^{-1} until 700 °C and it was maintained at this temperature for 6 h. Four mixed oxides catalysts were synthesized: $Ce_2Zr_2O_8$ (CZ) $Ce_2Zr_{1.5}Co_{0.47}O_{8-\delta}$ (CZCo), $Ce_2Zr_{1.5}Rh_{0.03}O_{8-\delta}$ (CZRh) and $Ce_2Zr_{1.5}Co_{0.47}Rh_{0.03}O_{8-\delta}$ (CZCoRh).

2.2. Catalytic tests

Glycerol steam reforming was performed in a straight tubular quartz reactor with a length of 30 cm. The description of the homemade rig was already reported [9]. For the reactivity tests, 55 mg of catalysts was diluted in 55 mg of silica carbide powder (SiC, supplied by SICAT®), both between 150 μm and 120 μm. Before the reaction, the catalysts were reduced in situ at 450 °C using 3 mL min^{-1} of pure H_2. The temperature was increased from room temperature to 450 °C at 2 °C min^{-1} and was maintained for 12 h. After reduction, the remaining H_2 was flushed out of the system using a mixture of inert gases (N_2:Ar). The temperature was then increased at 2 °C min^{-1} up to the reaction temperature of 650 °C. The reactant solution was a glycerol (SIGMA ALDRICH 99.0%):water mixture of 1:9 molar ratio, corresponding to 36 wt% of glycerol and 64 wt% of water. The reactant feed was pumped into the system using a Gilson 350 micropump at $0.0213 \, g_{solution} \, min^{-1}$ liquid flow, equivalent to 19 mL min^{-1} gas flow. The reactant mixture was diluted with 31 mL min^{-1} of N_2:Ar gas flow (1:4 molar ratio), and introduced into the reactor by a needle. N_2 was used as the internal standard for the quantification of the non-condensable products. All tests were performed over 24 h.

Two fractions of products were analyzed: non-condensable products (gaseous fraction) and condensable products (liquid fraction). The non-condensable products were quantified on-line every 30 min using gas chromatography (AGILENT TECH. 6890N Network GC system). H_2, CO, CO_2, CH_4 and C_2H_4 were analyzed using a Carbosieve II column. The condensable products were recovered from the exit reactor stream by two traps: the first one at room temperature and the second one at 0 °C. The liquid fraction recovery was performed three times: after 5 h, 8.5 h and 24 h. The condensable products were analyzed by chromatography (AGILENT TECH. 6890N Network GC system) on a ZB-Wax Plus (Zebron) column

using n-propanol as the internal standard. The liquid phase products analyzed were: acetone, acetaldehyde, acroleine, methanol, ethanol, hydroxyacetone, acetic acid, propionic acid, propylene glycol, ethylene glycol, glyceraldehyde and glycerol.

2.3. Analytical method

The parameters used to evaluate the performance of the catalysts in glycerol steam reforming were: global conversion of glycerol (X, Eq. (1)) that was calculated from the glycerol recovered from the liquid fraction; conversion to non-condensable products (X_G, Eq. (2)) and conversion to condensable products (X_L, Eq. (3)).

$$X(\%) = \left[1 - \frac{g_{Glycerol.out}}{g_{Glycerol.in}} \right] \times 100 \tag{1}$$

$$X_G(\%) - \frac{F_{CO_2} + F_{CO} + F_{CH_4} + 2F_{C_2H_4}}{3F_{Glycerol.in}} \times 100 \tag{2}$$

$$X_L(\%) = \frac{\Sigma F_i}{3F_{Glycerol.in}} \times 100 \tag{3}$$

where F_i represents the molar flow of the compound i; $g_{Glycerol.out}$ is the mass of exhaust glycerol recovered in the liquid fraction during a given interval of time, and $g_{Glycerol \, in}$ is the mass of glycerol introduced to the system during the same interval of time.

The conversions' values, presented in Table 3, are expressed as weighted mean with time. Those values were calculated taking into account the intervals of time selected to recover the condensable products. Eq. (4) shows the calculus of X_G between two different reaction times (t_1, t_2).

$$X_{G(t_1-t_2)}(\%) = \left[\frac{\sum_{t_1}^{t_2} X_G(t_i) \times \Delta t_i}{\sum_{t_1}^{t_2} \Delta t_i} \right] \times 100 \tag{4}$$

For the non-condensable products, a hydrogen balance was also calculated. The balance was expressed as the number of H-atoms present in the molecule of product (e.g. 4 in the case of CH_4 and C_2H_4), per mol of glycerol converted into non-condensable (gaseous phase) products (H-atoms$_G$ mol$_{Gly.Conv.Gas}{}^{-1}$).

The tendency of the catalysts to form carbon deposits during glycerol steam reforming was presented in the form of selectivity towards the formation of carbon (S_C), and was calculated as the ratio between the amount of carbon, obtained from TPO analysis, and the amount of carbon converted during the reaction (mmolC$_{total}$ mol$_{carbon-converted}{}^{-1}$).

2.4. Catalyst characterization

The crystalline structure of the mixed oxides catalysts were determined by XRD with a Brucker AXS-D8 Advanced equipment with Cu-Kα radiation ($\lambda = 1.5404$ Å). The 2θ range scatter used was 10–90° with a 0.05° step size at a scan rate of 3° min^{-1}.

High resolution transmission electron microscopy (HRTEM) observations were carried out using a TOPCON EM-002B apparatus (accelerating voltage 200 kV). Before analysis the samples were dispersed in toluene.

Raman Spectroscopy measurements were recorded in a dispersive Horiva Jobin Yvon LabRam HR800 Microscope, with a He–Ne green laser (532.14 nm) working at 5 mW, and with a 600 g mm^{-1} grating. The microscope used a 20× objective and a confocal pinhole of 150 μm. The Raman spectrometer was calibrated using a silicon wafer. Two types of measures were performed: (i) at room temperature under inert atmosphere and (ii) cycles of reduction-reoxidation using H_2 pure and synthetic air. In this last case a Linkam CCR100 cell was used coupled to the linked Raman equipment. The temperature was increased from room temperature to 550 °C at

$10\,°C\,min^{-1}$. The spectra were taken every $100\,°C$ after 15 min of stabilization [15].

Thermoprogrammed techniques: H_2-TPR and TPD-TPO characterizations were carried out using MICROMERITICS AUTO CHEM II 2920 equipment. For TPR and H_2-TPD characterizations, H_2 consumption was monitored by TCD detector. For the reoxidation capacity, the signals were followed by mass spectrometry using a PFEIFFER vacuum equipment coupled to a homemade piece of equipment. The characterization protocols are described hereafter:

TPR analyses were performed on 30 mg of fresh catalyst under $50\,mL\,min^{-1}$ of a 10% H_2/Ar mixture. The temperature was increased from room temperature up to $1000\,°C$ at $15\,°C\,min^{-1}$. The total H_2 consumption and the percentage of cerium reduced were calculated from the integration of TPR results. The H_2 consumption was discriminated by region and the corresponding percentage with respect to the global consumption was calculated. The percentage of reduced cerium (Ce^{4+} to Ce^{3+}) was determined assuming a total reduction of Co_3O_4 to Co^0, and Rh_2O_3 to Rh^0 [14].

TPD-TPO experiments were carried out on 20 mg of spent catalysts using $50\,mL\,min^{-1}$ of pure He in the desorption procedure, and $50\,mL\,min^{-1}$ of 10% O_2 diluted in Ar in the oxidation procedure. In both cases, the temperature was increased at $15\,°C\,min^{-1}$ from room temperature to $1000\,°C$. The $m/z = 16$, 18, 28, 32 and 44 signals were registered. However, the results are shown using the $m/z = 44$ (CO_2 signal).

The re-oxidation capacity of the fresh mixed oxides was estimated after a mild reduction treatment at $700\,°C$. The catalysts were reduced under $50\,mL\,min^{-1}$ of 1% H_2/He and then re-oxidized with 1% O_2/He. After the introduction of H_2/He mixture, the samples were heated at $15\,°C\,min^{-1}$ up to $700\,°C$ and then maintained for 1 h at this temperature. The H_2 consumption throughout this procedure was named $H_{2(TPR)}$. Desorption under helium was then carried out at room temperature. After desorption, the re-oxidation step was started. The introduction of O_2/He mixture was performed at room temperature until the stabilization of the signals. Then, the samples were again heated at $15\,°C\,min^{-1}$ up to $700\,°C$. The oxygen consumption upon heating was defined as $O_{2(TPO)}$. The $m/z = 2$, 16, 18, 28, 32 and 44 signals were registered. However, only the results of $m/z = 2$ and 32 (H_2 and O_2 signals, respectively) are shown.

3. Results

3.1. Fresh catalysts characterization

The characterization of the CZ, CZCo and CZCoRh catalysts by DRX and TPR has been previously published for the study of ethanol steam reforming [14,16]. As general conclusions it was established that the process of synthesis at the calcination temperature ($700\,°C$) allows the formation of fluorite type mixed oxides with a small segregation of cobalt oxide (Co_3O_4). In this case, as expected, for the four fresh mixed oxide, peaks of fluorite of cubic structure $Ce_{0.6}Zr_{0.4}O_2$ (JCPDS 38-1439) were observed at $2\theta = 29.1°$, $33.7°$, $48.5°$, $57.5°$, $60.4°$, $71.5°$ and $78.5°$ angles (Fig. 1). For CZCo and CZCoRh, the small diffraction peaks at $36.8°$ and $65.2°$, corresponding to Co_3O_4 spinel phase (JCPDS 43-1003), were also detected.

The crystalline structure of the catalysts was also verified by Raman spectroscopy (Fig. 2).

For CZ and CZRh mixed oxides only bands at 185, 303, 470 and $629\,cm^{-1}$ were observed. The main band at $470\,cm^{-1}$ corresponded to F_{2g} Raman active mode of fluorite type lattice [17,18]. The band at $303\,cm^{-1}$ has been attributed to the tetragonal substitution of oxygen atoms from the ideal fluorite lattice, while the band at $630\,cm^{-1}$ has been attributed to the presence of oxygen vacancies. The high
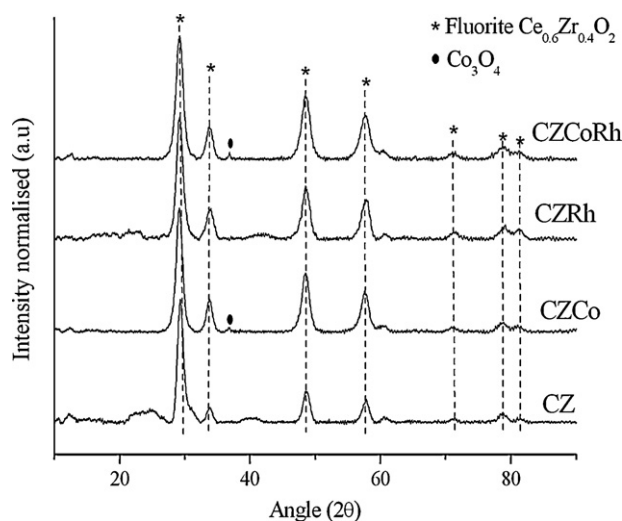

Fig. 1. X-ray diffraction patterns of fresh catalysts.

incorporation of Zr atoms in the ceria network generated a tetragonal phase-like distortion [19], which was observed in the intensity and location of these bands [20].

For the Co containing catalysts, bands at 191, 475, 517, 612 and $678\,cm^{-1}$ were noticed. These bands have been attributed to the cobalt spinel phase (Co_3O_4) [21], which typical bands are 191, 469, 512, 606 and $671\,cm^{-1}$. It was also observed that the peaks were shifted and broaded in different zones of the sample, indicating possible differences in the structure and particle size of the cobalt oxide.

The effect of Co and Rh on the reducibility of Ce-Zr mixed oxides was previously studied by TPR [14]. The presence of cobalt and rhodium favored the reduction of the Ce-Zr mixed oxide, lowering the temperature of reduction observed for the bare Ce-Zr. In the case of CZRh catalyst, the presence of Rh also favored the reduction in comparison to CZ (Fig. 3). The temperatures of maximal H_2 consumption were $297\,°C$ and $420\,°C$. The peak of higher intensity at $297\,°C$ can be related to the reduction of Rh^{3+} and surface Ce^{4+}. The peak at $420\,°C$ may be ascribed to the reduction of rhodium particles of different sizes [22] or rhodium particles with different interaction with the support.
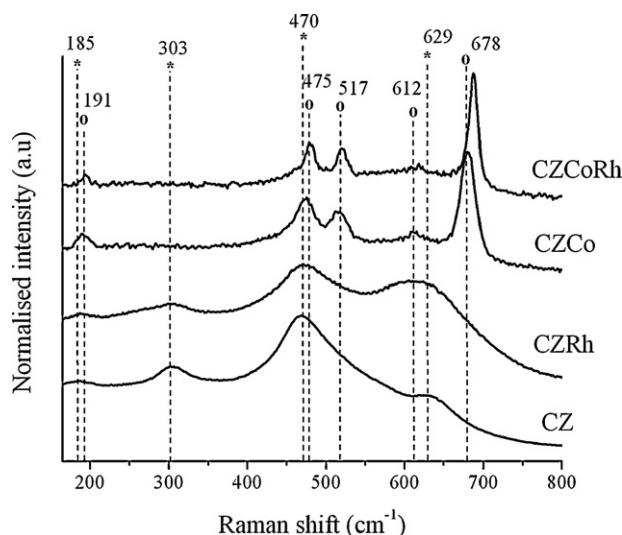

Fig. 2. Raman spectra of fresh CZ, CZRh, CZCo and CZCoRh at room temperature. Bands ascribed to the: (*) fluorite structure and (o) Co_3O_4 spinel structure.
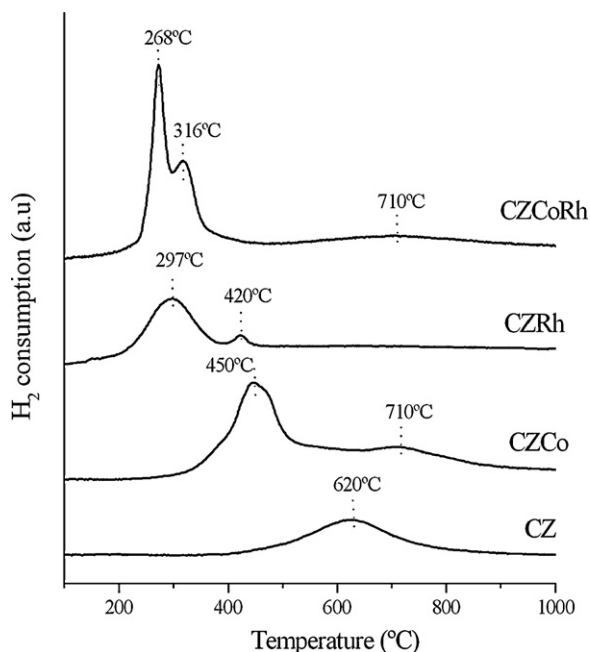
Fig. 3. H_2-TPR profiles of fresh catalysts.

Table 1
H_2 consumption for the fresh catalysts obtained from TPR results.

H_2 consumption (mmol H_2 $g_{cat.}^{-1}$).			
Total	Region I low temp.	Region II high temp.	% Ce reduced
0.76	0.00 (0%)	0.76 (100%)	45
1.97	0.91 (46%)	1.06 (54%)	45
0.90	0.52 (58%)	0.38 (42%)	48
2.72	1.20 (44%)	1.52 (56%)	88

The H_2 consumption and the percentage of reduced cerium are presented in Table 1. The total consumption of H_2 was increased for CZCo and CZRh compared to CZ. However, for both catalysts the increase of consumption corresponds only to the H_2 required to reduce the Co^{2+}/Co^{3+} to Co^0 for CZCo; or Rh^{3+} to Rh^0 for CZRh, since the percentage of reduced cerium (45% and 48% for Co and Rh catalysts, respectively) was similar to that calculated for CZ (45%). This result is in accordance with previous works where the overall degree of cerium reduction was only slightly affected by the presence of a metallic phase [23]. On the other hand, for CZCoRh, the total H_2 consumption was considerably increased by the simultaneous presence of Rh and Co. For CZCoRh, the cerium reduction was considerably higher (88%) than in the other catalysts (around 45%).

Table 2 presents the O_2 consumption calculated from the re-oxidation performed after mild reduction procedure ($O_{2(TPO)}$). The corresponding H_2 consumption during the reduction procedure is also shown ($H_{2(TPR)}$).

For all the catalysts, the amount of O_2 uptake during TPO increased along with the amount of H_2 consumed during TPR. This characteristic indicates the effective re-oxidation of the

Table 2
H_2 consumption and O_2 chemisorption in mild reduction procedure (700 °C) followed by TPO for CZ, CZCo, CZRh, and CZCoRh.

Catalysts	μmol H_2 $g_{catal.}^{-1}$ from $H_{2(TPR)}$	μmol O_2 $g_{catal.}^{-1}$ from $O_{2(TPO)}$	$O_{2(TPO)}/H_{2(TPR)}$
CZ	1468	742	0.50
CZCo	1854	930	0.50
CZRh	2020	1114	0.55
CZCoRh	2210	1173	0.53

samples, which was also verified by the $O_{2(TPO)}/H_{2(TPR)}$ ratio. For all the catalysts, $O_{2(TPO)}/H_{2(TPR)}$ was equal or higher than 0.5. This factor represents the stoichiometry between O_2 and H_2 to re-oxidize the catalyst. For CZRh and CZCoRh, the presence of rhodium favored the storage of oxygen. The amount of O_2 uptake was higher than the corresponding value for the mixed oxide re-oxidation ($O_{2(TPO)}/H_{2(TPR)} > 0.5$).

The structural changes with the increase in temperature under reductive and oxidative atmospheres were studied by in situ Raman spectroscopy for CZRh, CZCo and CZCoRh (Fig. 4).

For CZRh (Fig. 4a), the cubic structure was visible in reductive conditions up to 150 °C. Beyond this temperature the cubic structure was hardly noticeable. The cubic structure was reobserved when the temperature decreased to room temperature. Conversely, in oxidation conditions (Fig. 4b), the cubic structure was observed during the whole temperature range but the increase in temperature decreased the intensity of the peaks and changed the peaks' positions with respect to the original spectrum at room temperature. The initial position and the intensity of the cubic phase peaks were observed again when the temperature was decreased to room temperature.

For CZCo, the only visible phase at low temperature under reductive conditions was the spinel Co_3O_4 (Fig. 4c), as was previously observed in inert atmosphere (Fig. 2). The peaks of Co_3O_4 spinel were progressively less defined with the temperature increase and disappeared at 450 °C. After that, the fluorite cubic phase started to be noticeable. The peaks of cubic phase were well defined when the temperature was decreased to room temperature. Under synthetic air (Fig. 4d), the cubic phase remained visible. However, after 5 min the Co_3O_4 spinel phase started to be reobserved, although the peaks' position changed with respect to the initial spectra. Again, the definition of the Co_3O_4 spinel peaks decreased with the increase in temperature. Beyond 350 °C the spinel Co_3O_4 was poorly observed and the peaks corresponding to the ceria-zirconia cubic phase were observed. These peaks were well defined at 450 °C, but they disappeared at 550 °C. Finally, the initial Co_3O_4 spinel phase was characterized at the same peaks position when the temperature decreased to room temperature.

For CZCoRh, the Co_3O_4 spinel phase was always observed in reductive conditions at room temperature (Fig. 4e). Beyond 150 °C, the spinel phase disappeared and the peaks corresponding to the CZ cubic phase were observed. The peaks of the cubic phase were well defined and they remained until the temperature was decreased to room temperature. In contrast to the results observed with CZCo (Fig. 4d) the cubic phase was still noticed for CZCoRh (Fig. 4f) after changing to oxidative conditions, however, they disappeared with the increase in temperature. The cubic phase was visible again, after the temperature was decreased. However, the spinel Co_3O_4 phase was not recovered after the reduction-oxidation procedure.

According to the previous results, the presence of rhodium affected the behavior of the spinel Co_3O_4 phase observed in the CZCo catalyst. Rhodium inhibited the formation of Co_3O_4 at the surface after the reduction procedure, suggesting that Rh stabilizes the cobalt inserted in the fluorite structure or at least inhibits the cobalt rejection as Co_3O_4.

3.2. Activity results

Fig. 5 shows the evolution of H_2 production for 24 h of the reaction at 650 °C. This H_2 production was expressed as mol of H_2 produced per mol of glycerol introduced.

The H_2 production during the first hours of reaction was highly favored by the presence of Co and/or Rh. In addition the presence of Rh also favored the stability at high H_2 productions in comparison to the catalyst with only Co. For CZ oxide the maximal H_2 production was 0.8 mol H_2 $mol_{Gly.in}^{-1}$, while for CZCo it was

Fig. 4. Raman spectra of: (a) and (b) CZRh, (c) and (d) CZCo, and (e) and (f) CZCoRh during reduction and oxidation procedures. (●) fluorite structure and (★) Co_3O_4 spinel structure.

5 mol H_2 $mol_{Gly.in}^{-1}$, and for CZRh and CZCoRh the thermodynamic value (6.06 molH_2 $mol_{Gly.in}^{-1}$) was attained. However, for all the catalysts the H_2 production decreased with time on stream, reaching values lower than 1.2 mol H_2 $mol_{Gly.in}^{-1}$. The best performance was observed for the catalyst with both Co and Rh, where high H_2 productions close to thermodynamic value were obtained during approximately 8.5 h.

The evolution of global glycerol conversion (X), conversion to non-condensable products (X_G) and conversion to condensable products (X_L) is shown in Table 3. X, X_G and X_L are presented for the three periods of time of liquid fraction recovery (0–5 h, 5–8.5 h and 8.5–24 h).

It is shown that glycerol can be effectively transformed by all the catalysts. During the first 5 h of reaction, X was 89% for CZ and 100% for CZCo, CZRh and CZCoRh. Conversely, X_G and X_L significantly varied depending on the catalyst. For CZ, X_G was considerably low (35%) from the beginning of the reaction (0–5 h), and X_L was relatively high (12%) in comparison to the other catalysts ($X_L \leq 3\%$). This effect was better observed with the ratio X_L/X_G. The presence of Co decreased the ratio X_L/X_G favoring the production of non-condensable products over condensable products at the beginning of the reaction. For the catalysts with Rh, this effect was strongly accentuated; the lowest values of X_L/X_G were obtained over the whole test.

For all the catalysts X and X_G decrease with time on stream (Table 3), while X_L tends to increase in time.

The distribution of non-condensable products (H_2, CO_2, CO, CH_4 and C_2H_4) is presented in Fig. 6, expressed as mol of product per mole of glycerol converted into gaseous products. For CZ, the distribution of products was quite constant over the 24 h of reaction. For this catalyst, CO was the main product followed by C_2H_4 and H_2. The formation of CH_4 and CO_2 were also observed but in lower proportions. For CZCo, CZRh and CZCoRh, the main product was always H_2 followed by CO_2 and CO. In all cases, the formation of CH_4 was considerably low during the whole test (<0.23 mol CH_4 $mol_{Gly.Conv.gas}^{-1}$). For the three catalysts, the production of H_2 and CO_2 decreased along with the increase of the production of CO and C_2H_4. For CZCo and CZCoRh, two different reaction zones could be distinguished: the first one at high H_2
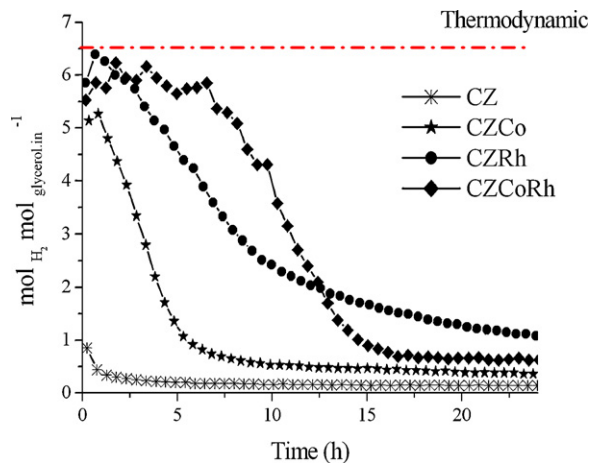

Fig. 5. Evolution of H_2 production, expressed as mol H_2 $mol_{glycerol.in}^{-1}$. Thermodynamic value: 6.06 mol H_2 $mol_{glycerol.in}^{-1}$ calculated using UNIQUAC model.

Table 3
Evolution with time of weighted mean conversions of glycerol at 650 °C.

	CZ			CZCo			CZRh			CZCoRh		
	0–5 h	5–8.5 h	8.5–24 h	0–5 h	5–8.5 h	8.5–24 h	0–5 h	5–8.5 h	8.5–24 h	0–5 h	5–8.5 h	8.5–24 h
X	89	67	55	100	100	56	100	100	68	100	96	64
X_G	35	27	22	71	30	19	94	70	37	97	92	37
X_L	11	13	13	3	12	9	0	3	6	0	3	6
X_L/X_G	0.30	0.47	0.58	0.04	0.40	0.49	0.00	0.05	0.15	0.00	0.04	0.15
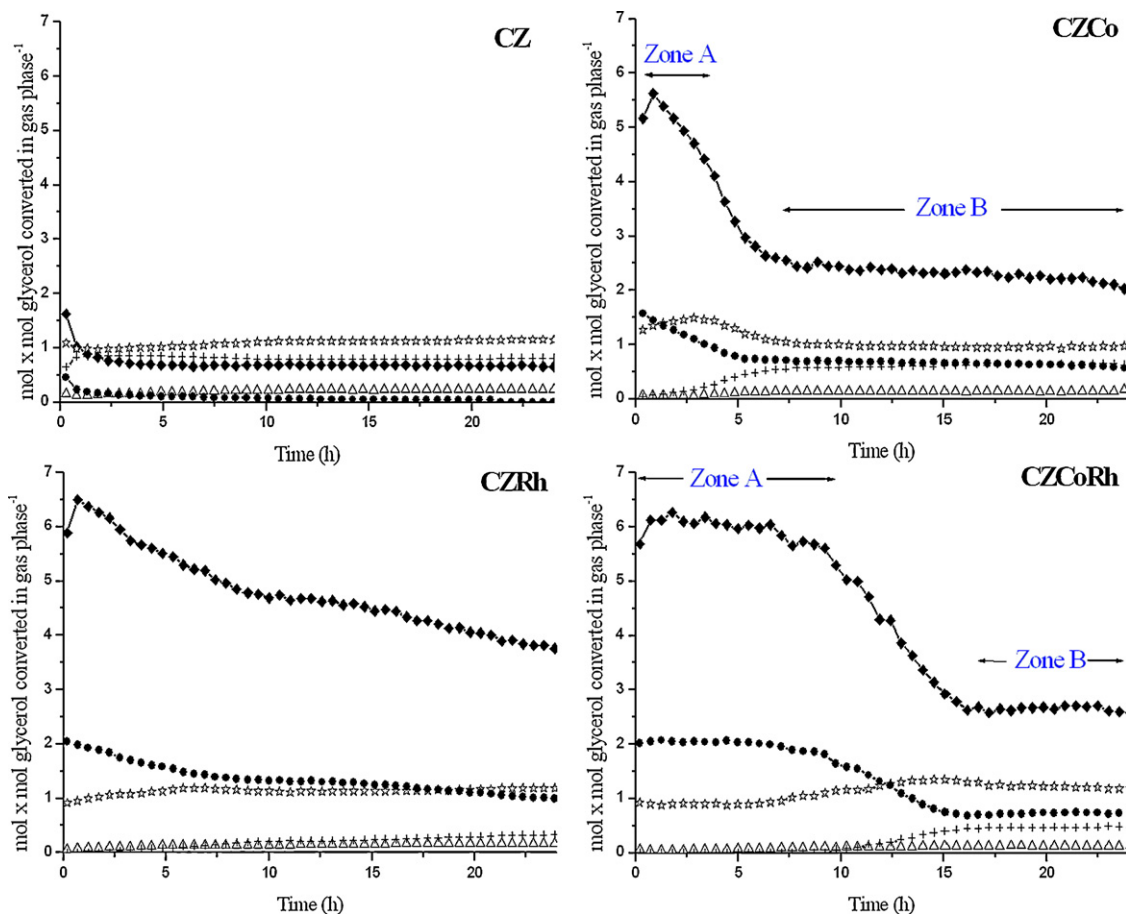
Fig. 6. Gas product distribution expressed as $mol_{compound}\, mol_{glycerol\ converted\ in\ gas\ phase}{}^{-1}$. Symbols: ♦ H_2, ☆ CO, △ CH_4, ● CO_2, + C_2H_4.

concentrations (>5 mol H_2 mol$_{Gly.Conv.gas}{}^{-1}$) and the second one at H_2 concentrations lower than 3 mol H_2 mol$_{Gly.Conv.gas}{}^{-1}$. In the first zone, called Zone A, the production of H_2 and CO_2 were favored while in the second zone, called Zone B, the production of C_2H_4, CO and CH_4 were increased.

The distribution of products (molar fractions) within the condensable fraction is presented in Table 4. For all the catalysts the principal product was hydroxyacetone, followed by the production of acetaldehyde, acrolein and methanol. Traces of acetic acid, propionic acid, ethylene glycol and acetone were also detected. For CZ and CZCo, the production of hydroxyacetone was favored with time on stream with the simultaneous decrease of the acetaldehyde production. For CZRh, the distribution of products was approximately constant after the first 5 h of reaction while for CZCoRh the formation of condensable products was only observed for the last period (8.5–24 h).

3.3. Spent catalyst characterization

After the steam reforming reaction the catalysts were characterized by the XRD, HRTEM and TPD-TPO experiments.

The XRD patterns of the spent catalysts (not shown) presented the characteristics peaks of the fluorite cubic structure ($Ce_{0.6}Zr_{0.4}O_2$ – JCPDS 38-1439) observed for the mixed oxides before test in Fig. 1. However, the peaks at 36.8° and 65.2°, corresponding to the Co_3O_4 spinel phase, were no longer observed for the Co containing catalysts.

Table 5 presents the comparison of the cubic lattice parameter "a" and the crystallite size for the four catalysts, before test (oxides) and after test. The cubic lattice parameter of the cubic phase-centred fluorite was calculated from the five most intense diffraction peaks [1 1 1], [2 0 0], [2 2 0], [3 1 1] and [2 2 2], and the crystallite size was determined according to the Debye–Scherrer equation from the full width at half maximum.

Before test, the cubic lattice parameter ("a") obtained for CZ and CZRh oxide was 5.28 Å. The presence of Co slightly increased "a" until 5.30 Å for CZCo and 5.29 Å for CZCoRh (Table 5). After test, "a" augmented for CZ, CZCo and CZCoRh. This enlargement of the cubic cell was more noticeable for CZCo, from 5.30 Å until 5.36 Å. Conversely, for CZRh "a" was slightly smaller after reaction indicating a contraction of the cubic cell.

Table 4
Evolution with time of condensable products (molar fraction) during GSR at 650 °C.

| Catalysts	CZ			CZCo			CZRh			CZCoRh		
Products (%)	0–5 h	5–8.5 h	8.5–24 h	0–5 h	5–8.5 h	8.5–24 h	0–5 h	5–8.5 h	8.5–24 h	0–5 h	5–8.5 h	8.5–24 h
Hydroxyacetone	38	50	61	44	53	63	0	54	57	0	0	63
Acetaldehyde	30	19	7	38	24	15	0	23	18	0	0	10
Acrolein	13	10	9	11	16	12	0	13	11	0	0	10
Methanol	9	9	9	0	2	0	0	10	8	0	0	5
Acetic acid	4	5	5	0	5	10	0	0	0	0	0	5
Propionic acid	3	2	3	0	0	0	0	0	2	0	0	0
Ehylene glycol	2	4	6	0	0	0	0	0	4	0	0	4
Acetone	1	0	0	7	0	0	0	0	0	0	0	0
Propylene glycol	0	0	0	0	0	0	0	0	0	0	0	4

Table 5
Cubic lattice parameters "a" and hydrogen consumption for the fresh catalysts obtained from XRD patterns before and after (*) glycerol steam reforming.

Catalysts	Cubic lattice "a" (Å)		Average crystallite size of CZ (nm)	
	Before	After	Before	After
CZ	5.28	5.30*	6.3	6.1*
CZCo	5.30	5.36*	6.0	6.1*
CZRh	5.28	5.27*	5.6	5.7*
CZCoRh	5.29	5.30*	5.4	5.4*

Table 6
Quantification of carbonaceous deposits after glycerol steam reforming.

Spent catalysts	mmol $C_{total} g_{catal.}^{-1}$	S_C (mmol C_{total} mol$_{carbon-converted}^{-1}$)
CZ	2.82	0.24
CZCo	2.62	0.20
CZRh	2.64	0.18
CZCoRh	1.50	0.10

HRTEM micrographs (Fig. 7) show the formation of superficial carbon and filamentous carbon for all the spent catalysts. The presence of cobalt seemed to favor the formation of filamentous carbon. For CZCo (Fig. 7b) the quantity of filaments appeared to be higher and more structured in comparison to the filaments observed with CZ (Fig. 7a) and the Rh-containing catalysts (Fig. 7c).

The formation of carbon deposits was also studied by the production of CO_2 during TPO experiments (Fig. 8). For all the spent catalysts, a peak of high intensity at 700 °C was observed. For CZCo and CZCoRh additional peaks were noticed at lowers temperatures. For CZCo at 531 °C, and for CZCoRh at 362 °C and 498 °C (zoom area of Fig. 8).

The quantification of carbon deposits from the TPO results are shown in Table 6. For CZ, the formation of carbon deposits was favored compared to the other catalysts (2.82 mmol $C_{total} g_{catal}^{-1}$). The presence of Co or Rh slightly decreased these formations to 2.62 mmol $C_{total} g_{catal}^{-1}$ and 2.64 mmol $C_{total} g_{catal}^{-1}$, respectively. For CZCoRh, the simultaneous presence of Co and Rh significantly decreased the amount of carbon deposits (1.50 mmol $C_{total} g_{catal}^{-1}$).
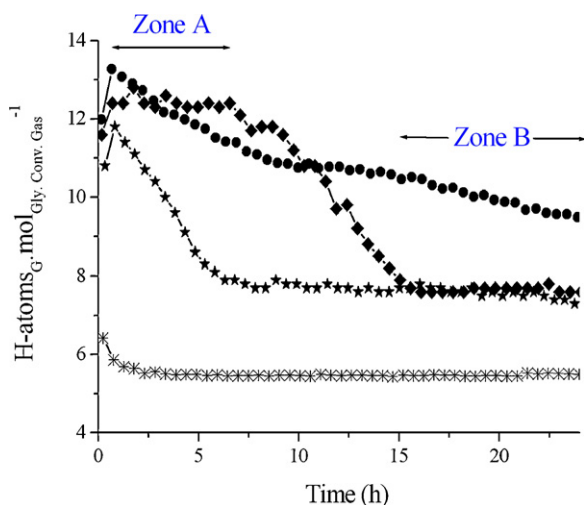
Fig. 7. HRTEM micrographs of: (a) CZ, (b) CZCo and (c) CZCoRh catalysts after glycerol steam reforming.

The selectivity towards the formation of carbon deposits (S_C: mmol C_{total} mol$_{carbon-converted}^{-1}$) is also presented in Table 6. The reduction in the formation of carbon deposits was more evident according to this parameter: for bare CZ catalyst, S_C was 0.24 mmol C_{total} mol$_{carbon-converted}^{-1}$. For CZCo and CZRh, S_C was reduced until 0.20 and 0.18 mmol C_{total} mol$_{carbon-converted}^{-1}$, respectively. This effect was considerably pronounced when both metals, Co and Rh, were present in the catalyst, where Sc was only 0.10 mmol C_{total} mol$_{carbon-converted}^{-1}$.

4. Discussion

4.1. Effect of the catalyst

According to reactivity results, it is clear that glycerol conversion can be performed using CZ, CZCo, CZRh and CZCoRh catalysts (Table 3). However, it was also observed that even at high glycerol conversions the production of H_2 can be considerably low, like for CZ (Fig. 5). The presence of Co considerably increased the production of H_2, and this effect was even stronger when CZRh was used. According to this, the selective production of H_2 in glycerol steam reforming requires the presence of a metallic phase, like Co or Rh.

The better performance of CZRh in comparison to CZCo could be related to the higher capacity of Rh to activate the C—C bond [24,25]. But also to the enhanced oxygen storage of CZRh in comparison to CZCo (higher $O_{2(TPO)}/H_{2(TPR)}$ ratio in Table 2).

On the other hand, CZCoRh catalyst showed the best results with higher H_2 productions for a longer reaction time (Fig. 5). This catalyst presented the highest percentage of cerium reduced, importantly higher in comparison to CZCo and CZRh (Table 1), and the oxygen storage was enhanced compared to CZCo (Table 2).The promotion of the reducibility and re-oxidation properties of the catalyst seemed to promote the catalytic behavior, inhibiting the faster deactivation observed for CZCo and CZRh.

In ethanol steam reforming using Co supported on SiO_2 and CeO_2–ZrO_2, it was observed that the presence of Rh enhance the stability of the catalyst [22,26]. It was concluded that Rh would prevent the cobalt oxidation, acting as a nucleation centre "catalyzing" the reduction of Co [27,28].

By in situ Raman Spectroscopy, it was also noticed that Rh stabilizes Co in the mixed oxide (Fig. 4). Rhodium affected the behavior of cobalt in the mixed oxide matrix, avoiding the formation of Co_3O_4 at the surface after reduction. The presence of Rh could either
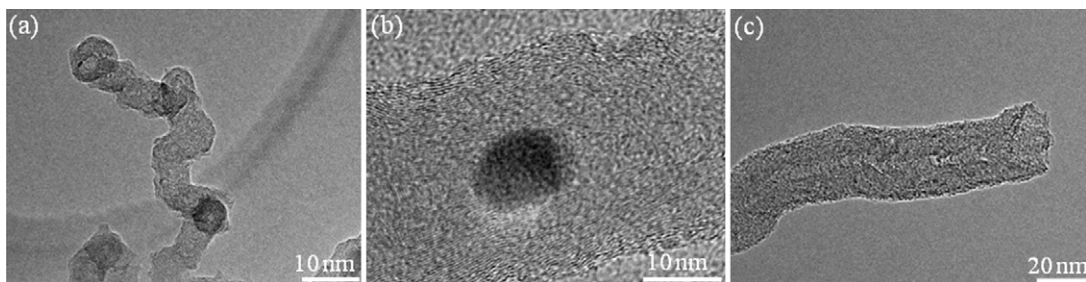
Fig. 8. TPO profiles after glycerol reforming. Magnification on spent CZCo and CZCoRh.

stabilize the cobalt inserted in the fluorite structure or inhibit the cobalt rejection as Co_3O_4. These effects could also favor the stability of CZCoRh under reaction conditions.

The deactivation of the catalysts was observed in the decrease of H_2 yield and global glycerol conversion (X), but also by the increase of the X_L/X_G ratio and the variation of the distribution of non-condensable products.

For the CZ catalyst, no significant signs of deactivation were observed besides the decrease of X with time of reaction. For this catalyst, the H_2 production was always relatively low compared to the other catalysts and the proportion of X_L/X_G was always relatively high. The principal non-condensable products were CO and C_2H_4, followed by H_2 and CH_4 in lower proportions. Stein et al. [29] studied the pyrolysis of glycerol in steam at 650 °C. The initial products observed were CO, acetaldehyde and acrolein. Acetaldehyde and acrolein further decomposed to produce mainly CO, C_2H_4, CH_4 and H_2. In more recent studies in glycerol steam reforming, Chiodo et al. [30] have also reported that glycerol drastically decomposes at temperatures higher than 447 °C. The formation of CO (>50%), C_2H_4 (25%), CH_4 (13%), H_2 (10%) and traces of CO_2 (1%) were observed. Thus, glycerol could have thermally decomposed under the actual reaction conditions (650 °C), producing mainly non-condensable products.

In order to establish the effective participation of H_2O in the reaction, an H-atoms balance was performed for the non-condensable products (H_2, CO_2, CO, CH_4 and C_2H_4). For glycerol steam reforming, according to Reaction (1), the balance of H-atoms will be the 8H-atoms coming from the glycerol molecule ($C_3H_8O_3$) and 6H-atoms coming from the 3 molecules of water (14H-atoms). For glycerol decomposition (Reaction (2)), only 8H-atoms from glycerol will appear.

For CZ, the balance of H-atoms remained at 6H-atoms$_G$ mol$_{Gly.Conv.Gas}^{-1}$ during the whole test (Fig. 9). On the other hand, for CZCo, CZRh and CZCoRh, the balance of H-atoms was higher than 12H-atoms$_G$ mol$_{Gly.Conv.gas}^{-1}$, at the beginning of the test. This indicates the participation of H_2O in the formation of the non-condensable products for the latter. For the CZ catalyst the activity to glycerol conversion and the low selectivity towards H_2 is then related not to a catalytic effect of CZ but to a thermal decomposition of glycerol favored at the reaction temperature (650 °C).

For CZRh, CZCo and CZCoRh, the balance of H-atoms decreased progressively. For CZRh, it decreased progressively from 13 to 10H-atoms$_G$ mol$_{Gly.Conv.Gas}^{-1}$. For CZCo and CZCoRh, two regions of stability were noticed, like for the distribution of non-condensable products: Zone A, at high H-atoms balance (12H-atoms$_G$ mol$_{Gly.Conv.Gas}^{-1}$); and Zone B, at low H-atoms balance (8H-atoms$_G$ mol$_{Gly.Conv.G}^{-1}$). According to this, during the last period of time or Zone B (8.5–24 h), CZCo, CZRh and CZCoRh would progressively lose their ability to activate H_2O and the H-atoms balance will approach the balance observed with CZ (glycerol decomposition).

The differences between the catalysts could be then related to the capacity to activate H_2O under the reaction conditions, reason why the redox properties were highly influent in the catalytic behavior. Dou et al. [31] have already introduced this idea in glycerol steam reforming, where the catalyst's performance should be estimated according to H_2O conversion and not to glycerol conversion.

The characterization of the catalysts after test showed two possible deactivation causes: (i) changes in the fluorite structure (enlargement of the cubic cell – "a" (Table 5), and (ii) the formation of carbon deposits.

It has been proven by XANES [32] that cobalt can be inserted under the form of Co^{2+} in Ce-Zr fluorite type oxides by an appropriate method of synthesis. Co^{2+} is inserted in octahedral coordination, modifying the local environment of Ce^{4+} and Zr^{4+} cations. The rejection of cobalt from the fluorite structure during reaction will cause an enlargement of cubic cell. The ionic radii of Co^{2+} (0.73 Å) is smaller than the ionic radii of Ce^{3+} (1.14 Å), Ce^{4+} (1.97 Å), or Zr^{4+} (0.84 Å), therefore any rejection of Co^{2+} from the fluorite will lead to cell enlargement, like it was observed for CZCo catalyst (Table 5). For CZCoRh the expansion of the cubic cell was smaller in comparison to CZCo. The rejection of cobalt would be prevented by the action of Rh. This is in agreement with the previously discussed stabilizing effect of Rh.
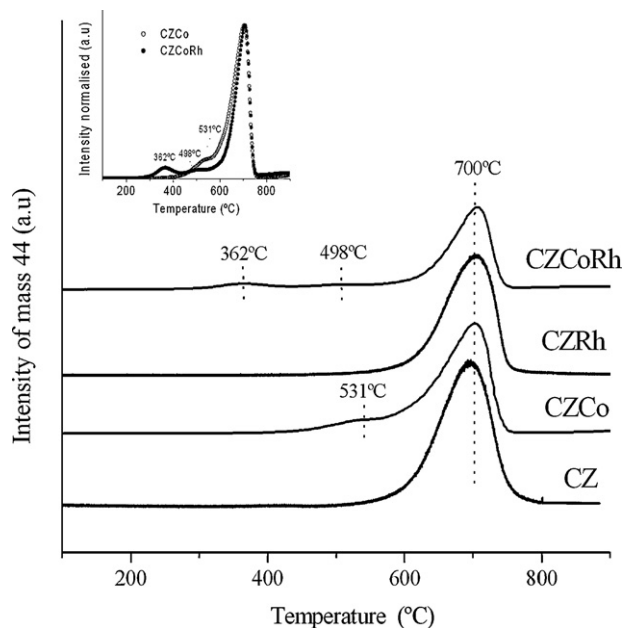

Fig. 9. Balance of the H-atoms contained in the non-condensable products per mole of glycerol converted in gaseous phase using (✷) CZ, (★) CZCo, (●) CZRh and (♦) CZCoRh.

The formation of surface carbon and carbon filaments was observed on spent catalysts by HRTEM (Fig. 7), and also by the formation of several peaks ascribed to carbon deposits observed in TPO analysis (Fig. 8). Surface carbon and filamentous carbon can be oxidized at different temperatures. Lower temperatures are mostly ascribed to surface carbon, while higher temperatures are ascribed to the oxidation of filamentous carbon [33,34]. All catalysts showed a similar oxidation peak at higher temperatures indicating the presence of filamentous carbon. According to the HRTEM results, the presence of Co seemed to favor the formation of carbon filaments more than CZ and CZRh catalysts.

Conversely, the different oxidation temperatures in TPO have also been related to the oxidation of carbon deposits in different locations on the catalyst surface [35–37]. The peak at 700 °C could be then ascribed to carbon or adsorbed species deposited over the support, while the peaks at lower temperatures (<500 °C), observed for CZCo and CZCoRh, can be related to carbon deposits formed close to metallic particles. The presence of the metal particle would favor the oxidation at lower temperatures [35].

The presence of Co decreases the formation of carbon deposits in comparison to the bare CZ catalyst. This effect was stronger with Rh and even stronger with the simultaneous presence of Co and Rh. The presence of Co and Rh would inhibit the formation of carbon deposits or/and would facilitate the gasification of the carbon deposits formed during reaction. Therefore, the higher performance of CZCoRh would be related to a cooperative effect between Co and Rh that: (i) promotes the redox properties avoiding the accumulation of carbon deposits by gasification, and (ii) stabilizes cobalt under reaction conditions thanks to Rh presence.

4.2. Reaction pathway

The reactivity results and the characterization after testing showed the formation of several products and carbon deposits during glycerol steam reforming. According to the reactivity results, the same non-condensable and condensable products were observed for the four catalysts. Therefore a similar reaction pathway can be proposed following the different trends observed during the reaction.

In the case of non-condensable products H_2, CO_2, CO will be formed by glycerol steam reforming (Reaction (1)) or by coupling glycerol decomposition (Reaction (2)) to WGSR (Reaction (3)).

$$C_3H_8O_3 + 3H_2O \rightarrow 3CO_2 + 7H_2 \tag{1}$$

$$C_3H_8O_3 \rightarrow 3CO + 4H_2 \tag{2}$$

$$CO + H_2O \Leftrightarrow CO_2 + H_2 \tag{3}$$

CH_4 formation would proceed by methanation reaction (Reaction (4)), with the coupling of H_2 and CO formed by glycerol decomposition.

$$CO + 3H_2 \Leftrightarrow CH_4 + H_2O \tag{4}$$

In the case of condensable products, the main products were hydroxyacetone, acetaldehyde, acrolein and methanol (Table 4). Hydroxyacetone and acrolein have been reported as the main products of glycerol dehydration [38] (Reaction (5) and (6), respectively). The formation of acetaldehyde can proceed according to Reaction (7) [39,40], with the simultaneous formation of formaldehyde and water. The formation of methanol has been reported in ethylene glycol reforming, as a product of ethylene glycol hydrogenation followed by irreversible C—C bond cleavage [41]. For glycerol steam reforming the equivalent of this reaction could be represented by Reaction (8). Bûhler et al. [42] also reported the production of methanol from glycerol pyrolysis by Reaction (9).

$$C_3H_8O_3 \rightarrow CH_3C(O)CH_2OH + H_2O \tag{5}$$

$$C_3H_8O_3 \rightarrow CH_2 = CHCHO + 2H_2O \tag{6}$$

$$C_3H_8O_3 \rightarrow HCHO + CH_3CHO + H_2O \tag{7}$$

$$C_3H_8O_3 + 3/2H_2 \rightarrow 3CH_3OH \tag{8}$$

$$C_3H_8O_3 \rightarrow 2HCHO + CH_3OH \tag{9}$$

The formation of acetic acid was also observed but in lower proportions. Its production proceeds according to Reaction (10) [43], as was previously defined.

$$CH_3CHO + H_2O \rightarrow CH_3COOH + H_2 \tag{10}$$

The apparition of C_2H_4 after deactivation could be related to further transformation of acetaldehyde according to Reaction (11)
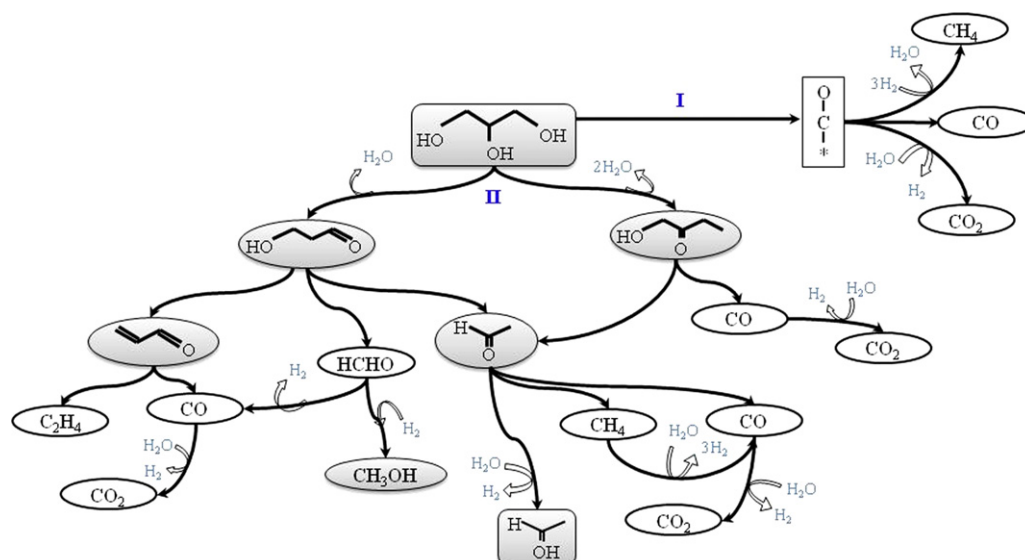
Fig. 10. Schema of reaction pathways in glycerol steam reforming.

[43], and/or via decarbonylation of acrolein [44–46] following Reaction (12).

$$CH_3CHO + H_2 \rightarrow C_2H_4 + H_2O \qquad (11)$$

$$CH_2 = CHCHO \rightarrow CO + C_2H_4 \qquad (12)$$
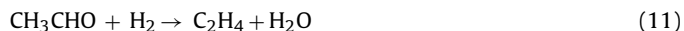
Adhikari et al. [43] published a reaction scheme for glycerol steam reforming, considering the experimental observation performed in several experimental works. The reaction scheme involved the direct formation of hydroxyacetone ($C_3H_6O_2$), acrolein (C_3H_4O), acetaldehyde (CH_3CHO) and formaldehyde (HCHO) by dehydration steps. The formation of CH_4, CO and CO_2 was presented by direct decomposition of glycerol and subsequent WGS reaction. Nevertheless, the dehydration of glycerol has also been reported to produce hydroxyacetone and 3-hydroxypropenal as primary products. 3-hydroxypropenal is a very unstable product that can lead to the formation of either acrolein or the acetaldehyde along with a molecule of formaldehyde [47].

According to the different observations during the reaction and the discussion above, the reaction scheme presented in Fig. 10 is proposed for glycerol steam reforming. Two main reactions' routes were considered: Route (I) represented the direct conversion of glycerol to the principal non-condensable products (H_2, CO_2, CO and CH_4); and Route (II) presented the formation of condensable products and then the formation of H_2, CO_2, CO and CH_4 by different subsequent reactions.

From Route (I), H_2, CO_2, CO and CH_4 would be directly formed from glycerol. From Route (II), the formation of hydroxyacetone and 3-hydroxypropenal would proceed by glycerol dehydration, and the formation of acrolein and acetaldehyde would take place by the subsequent decomposition of 3-hydroxypropenal. From the previous products, the formation of C_2H_4 (Reaction (12)), acetic acid (Reaction (10)) and methanol (Reaction (9)) is possible. The formation of methanol has been also related to the formation of 3-hydroxypropenal [40,47]. Chai et al. [40] reported that 3-hydroxypropenal decomposes in acetaldehyde and formaldehyde by reversed aldol condensation. Formaldehyde would further decompose producing CO and H_2 (Reaction (13)), and by hydrogenation it would lead to the formation of CH_3OH (Reaction (14)).

$$HCHO \rightarrow CO + H_2 \qquad (13)$$

$$HCHO + H_2 \rightarrow CH_3OH \qquad (14)$$

The formation of non-condensable products (H_2, CO_2, CO and CH_4) could also proceed by the steam reforming or further decomposition of these condensable products.

The simultaneous decrease of X_G and the increase of X_L with time on stream (Fig. 7) indicated that either Route (II) started to be favored over Route (I), or that the catalyst progressively lost the capacity to activate water, thus to further reform the non-condensable products into H_2, CO_2, CO, and CH_4.

The formation of carbon deposits can be also related to the formation of hydroxyacetone and acrolein. For acrolein, the production of coke has been reported by further dehydration of the molecule [47]; and for hydroxyacetone, it has been reported that it can oligomerise to form polyglycerol species, which may lead to coking reactions [48].

5. Conclusions

The catalytic behavior of ceria-zirconia mixed oxides was evaluated in the selective H_2 production by glycerol steam reforming. It was observed that glycerol conversion can be effective for CZ, CZRh, CZCo and CZCoRh catalysts. However, selective H_2 production requires a metallic phase.

The enhancement in the redox behavior, favored the catalytic performance for the H_2 production by glycerol steam reforming.

The presence of Co and Rh enhanced the redox properties of CZ. The simultaneous presence of Co and Rh enhanced these properties even more, an effect that encouraged the high production of H_2 for a longer period of time. The presence of both Co and Rh seemed to favor the gasification of the carbon deposits formed during reaction.

The catalytic performance was related to the redox properties of the catalysts and therefore to its capacity to activate H_2O under the reaction conditions.

According to the different by-products a global reaction system was proposed with two main reaction routes: (I) the direct glycerol steam reforming with the direct production of non-condensable products, and/or (II) the formation of condensable products with the subsequent steam reforming to produce non-condensable products.

Acknowledgments

References

[1] M. Pagliaro, R. Ciriminna, H. Kimura, M. Rossi, C. Della Pina, Angewandte Chemie International 46 (2007) 4434–4440.
[2] M. Slinn, K. Kendall, C. Mallon, J. Andrews, Bioresource Technology 99 (2008) 5851–5858.
[3] P. Ramirez de la Piscina, N. Homs, Chemical Society Reviews 37 (2008) 2459–2467.
[4] P.D. Vaidya, A.E. Rodrigues, Chemical Engineering & Technology 32 (2009) 1463–1469.
[5] T. Hirai, N.o. Ikenaga, T. Miyake, T. Suzuki, Energy and Fuels 19 (2005) 1761–1762.
[6] B. Zhang, X. Tang, Y. Li, Y. Xu, W. Shen, International Journal of Hydrogen Energy 32 (2007) 2367–2373.
[7] S. Adhikari, S. Fernando, A. Haryanto, Catalysis Today 129 (2007) 355–364.
[8] S. Adhikari, S.D. Fernando, S.D.F. To, R.M. Bricka, P.H. Steele, A. Haryanto, Energy and Fuels 22 (2008) 1220–1226.
[9] M. Araque, L.M. Martinez T, J.C. Vargas, A.C. Roger, Catalysis Today 176 (2011) 352–356.
[10] V. Nichele, M. Signoretto, F. Menegazzo, A. Gallo, V. Dal Santo, G. Cruciani, G. Cerrato, Applied Catalysis B: Environmental 111–112 (2012) 225–232.
[11] C.D. Dave, K.K. Pant, Renewable Energy 36 (2011) 3195–3202.
[12] J.C. Vargas, S. Libs, A.-C. Roger, A. Kiennemann, Catalysis Today 107–108 (2005) 417–425.
[13] F. Romero-Sarria, J.C. Vargas, A.-C. Roger, A. Kiennemann, Catalysis Today 133–135 (2008) 149–153.
[14] M. Araque, J.C. Vargas, Y. Zimmermann, A.C. Roger, International Journal of Hydrogen Energy 36 (2011) 1491–1502.
[15] W.Y. Hernandez, F. Romero-Sarria, M.A. Centeno, J.A. Odriozola, The Journal of Physical Chemistry C 114 (2010) 10857–10865.
[16] M. Virginie, M. Araque, A.-C. Roger, J.C. Vargas, A. Kiennemann, Catalysis Today 138 (2008) 21–27.
[17] M. Yashima, K. Morimoto, N. Ishizawa, M. Yoshimura, The Journal of the American Ceramic Society 76 (1993) 1745–1750.
[18] S. Damyanova, B. Pawelec, K. Arishtirova, M.V.M. Huerta, J.L.G. Fierro, Applied Catalysis A 337 (2008) 86–96.
[19] E. Fernandez Lopez, V. Sanchez Escribano, M. Panizza, M.M. Carnasciali, G. Busca, Journal of Materials Chemistry 11 (2001) 1891–1897.
[20] L. Liu, Z. Yao, B. Liu, L. Dong, Journal of Catalysis 275 (2010) 45–60.
[21] J. Jiang, L. Li, Materials Letters 61 (2007) 4894–4896.
[22] E.B. Pereira, N. Homs, S. Martí, J.L.G. Fierro, P. Ramírez de la Piscina, Journal of Catalysis 257 (2008) 206–214.
[23] C. De Leitenburg, A. Trovarelli, J. Kašpar, Journal of Catalysis 166 (1997) 98–107.
[24] M.A. Vannice, Journal of Catalysis 37 (1975) 449–461.
[25] R.R. Davda, J.W. Shabaker, G.W. Huber, R.D. Cortright, J.A. Dumesic, Applied Catalysis B 43 (2003) 13–26.
[26] E.B. Pereira, P. Ramirez de la Piscina, S. Marti, N. Homs, Energy and Environmental Science 3 (2010) 487–493.
[27] H.F.J. van't Blik, R. Prins, Journal of Catalysis 97 (1986) 188–199.
[28] J.H.A. Martens, H.F.J. Van't Blik, R. Prins, Journal of Catalysis 97 (1986) 200–209.
[29] Y.S. Stein, J.M.J. Antal, j.M. Jones, Journal of Analytical and Applied Pyrolysis 4 (1983) 283–296.
[30] V. Chiodo, S. Freni, A. Galvagno, N. Mondello, F. Frusteri, Applied Catalysis A: General 381 (2010) 1–7.

[31] B. Dou, V. Dupont, G. Rickett, N. Blakeman, P.T. Williams, H. Chen, Y. Ding, M. Ghadiri, Bioresource Technology 100 (2009) 3540–3547.

[32] E. Ambroise, C. Courson, A.C. Roger, A. Kiennemann, G. Blanchard, S. Rousseau, X. Carrier, E. Marceau, C. La Fontaine, F. Villain, Catalysis Today 154 (2010) 133–141.

[33] D.L. Trimm, Catalysis Today 49 (1999) 3–10.

[34] C.H. Bartholomew, Catalysis Reviews 24 (1982) 67–112.

[35] D. Duprez, M. Hadj-Aissa, J. Barbier, Applied Catalysis 49 (1989) 67–74.

[36] F.B. Noronha, E.C. Fendley, R.R. Soares, W.E. Alvarez, D.E. Resasco, Chemical Engineering Journal 82 (2001) 21–31.

[37] S.M. de Lima, A.M. Silva, U.M. Graham, G. Jacobs, B.H. Davis, L.V. Mattos, F.B. Noronha, Applied Catalysis A 352 (2009) 95–113.

[38] C.-H. Zhou, J.N. Beltramini, Y.-X. Fan, G.Q. Lu, Chemical Society Reviews 37 (2008) 527–549.

[39] M.R. Nimlos, S.J. Blanksby, X. Qian, M.E. Himmel, D.K. Johnson, Journal of Physical Chemistry A 110 (2006) 6145–6156.

[40] S.-H. Chai, H.-P. Wang, Y. Liang, B.-Q. Xu, Green Chemistry 9 (2007) 1130–1136.

[41] J.W. Shabaker, J.A. Dumesic, Industrial & Engineering Chemistry Research 43 (2004) 3105–3112.

[42] W. Bühler, E. Dinjus, H.J. Ederer, A. Kruse, C. Mas, The Journal of Supercritical Fluids 22 (2002) 37–53.

[43] S. Adhikari, S.D. Fernando, A. Haryanto, Energy Conversion and Management 50 (2009) 2600–2604.

[44] N.F. Brown, M.A. Barteau, Journal of the American Chemical Society 114 (1992) 4258–4265.

[45] R. Shekhar, M.A. Barteau, Surface Science 319 (1994) 298–314.

[46] A. Corma, G.W. Huber, L. Sauvanaud, P. O'Connor, Journal of Catalysis 247 (2007) 307–327.

[47] A. Corma, G.W. Huber, L. Sauvanaud, P. O'Connor, Journal of Catalysis 257 (2008) 163–171.

[48] J. Barrault, J.M. Clacens, Y. Pouilloux, Topics in Catalysis 27 (2004) 137–142.